

1 **An efficient arabinoxylan-debranching α -L-arabinofuranosidase of family GH62 from *Aspergillus nidulans***
2 **contains a secondary carbohydrate binding site**

3
4 Casper Wilkens^{1,A}, Susan Andersen¹, Bent O. Petersen^{2,B}, An Li³, Marta Busse-Wicher³, Johnny Birch¹, Darrell
5 Cockburn^{1,C}, Hiroyuki Nakai^{1,D}, Hans E. M. Christensen⁴, Birthe B. Kragelund⁵, Paul Dupree³, Barry McCleary⁶, Ole
6 Hindsgaul², Maher Abou Hachem¹ and Birte Svensson^{1,*}

7
8 ¹Enzyme and Protein Chemistry, Department of Systems Biology, Technical University of Denmark, Elektrovej,
9 Building 375, DK-2800 Kgs. Lyngby, Denmark

10 ²Carbohydrate Chemistry Group, Carlsberg Laboratory, Gamle Carlsberg Vej 10, DK-1799 Copenhagen V, Denmark

11 ³Department of Biochemistry, University of Cambridge, Tennis Court Road, Cambridge CB2 1QW, UK

12 ⁴Metalloprotein Chemistry and Engineering, Department of Chemistry, Technical University of Denmark, Kemitorvet,
13 Building 207, DK-2800 Kgs. Lyngby, Denmark

14 ⁵Structural Biology and NMR Laboratory, Department of Biology, University of Copenhagen, Ole Maaloes Vej 5, DK-
15 2200 Copenhagen N, Denmark

16 ⁶Megazyme International, Bray Business Park, Bray, Co. Wicklow, Ireland

17 *To whom correspondence should be addressed: Enzyme and Protein Chemistry, Department of Systems Biology,
18 Technical University of Denmark, Elektrovej, Building 375, DK-2800 Kgs. Lyngby, Denmark, Tel.: +45 4525 2740, E-
19 mail: bis@bio.dtu.dk

20 ^APresent address: Department of Chemical and Biochemical Engineering, Technical University of Denmark, Søtofts
21 Plads, Building 227, DK-2800 Kgs. Lyngby, Denmark

22 ^BPresent address: Biophysics and Biotechnology, Novo Nordisk A/S, Novo Nordisk Park, DK-2760, Måløv, Denmark

23 ^CPresent address: Department of Microbiology and Immunology, University of Michigan Medical School, Ann Arbor,
24 MI 48109, Michigan, U.S.A.

25 ^DPermanent address: Graduate School of Science and Technology, Niigata University, 8050 Ikarashi, Nishi-ku, Niigata
26 950-2181, Japan

27
28 **Abstract:** An α -L-arabinofuranosidase of GH62 from *Aspergillus nidulans* FGSC A4 (*AnAbf62A*-m2,3) has unusually
29 high activity towards wheat arabinoxylan (WAX) (67 U/mg; $k_{\text{cat}} = 178 \text{ s}^{-1}$, $K_{\text{m}} = 4.90 \text{ mg/ml}$) and
30 arabinoxylooligosaccharides (AXOS) with degree of polymerisation (DP) 3–5 (37–80 U/mg), but about 50 times
31 lower activity for sugar beet arabinan and 4-nitrophenyl- α -L-arabinofuranoside. α -1,2- and α -1,3-linked
32 arabinofuranose is released from mono-, but not from disubstituted xylose in WAX and different AXOS as
33 demonstrated by NMR and polysaccharide analysis by carbohydrate gel electrophoresis (PACE). Mutants of the
34 predicted general acid (Glu¹⁸⁸) and base (Asp²⁸) catalysts, and the general acid pK_a modulator (Asp¹³⁶) lost 1700-, 165-
35 and 130-fold activity for WAX. WAX, oat spelt xylan, birchwood xylan and barley β -glucan retarded migration of
36 *AnAbf62A*-m2,3 in affinity electrophoresis (AE) although the two latter are neither substrates nor inhibitors. Trp²³ and
37 Tyr⁴⁴, situated about 30 Å from the catalytic site as seen in an *AnAbf62A*-m2,3 homology model generated using
38 *Streptomyces thermoviolaceus* *SthAbf62A* as template, participate in carbohydrate binding. Compared to wild-type,
39 W23A and W23A/Y44A mutants are less retarded in AE, maintain about 70 % activity towards WAX with K_{i} of WAX

40 substrate inhibition increasing 4–7 fold, but lost 77–96 % activity for the AXOS. The Y44A single mutant had less
41 effect suggesting Trp²³ is a key determinant. *AnAbf62A-m2,3* seems to apply different polysaccharide-dependent
42 binding modes and Trp²³ and Tyr⁴⁴ belong to a putative surface binding site which is situated at a distance of the active
43 site and has to be occupied to achieve full activity.

44

45 **Keywords:** Glycoside hydrolase family 62, Inverting mechanism, Arabinoxylan, Arabinoxylooligosaccharides, Affinity
46 gel electrophoresis, Surface binding site

47

48 **Introduction**

49

50 Plants supply the most abundant biomass on earth and sustainable utilisation of this renewable resource is very
51 important for society. Plant cell walls are rich in L-arabinofuranose (Araf) found in arabinan main chains, pectin side
52 chains and as decorations of arabinoxylan (AX), arabinogalactan and gum arabic. Removal of Araf residues constitutes
53 a bottleneck in plant biomass conversion (Jordan et al. 2012) and efficient α -L-arabinofuranosidases (ABFs) (EC
54 3.2.1.55) are needed for various industrial processes such as bioethanol production (Numan and Bhosle 2006).

55 ABFs occur in glycoside hydrolase families GH3, 43, 51, 54 and 62 of the Carbohydrate Active Enzymes database
56 (CAZy) (Lombard et al. 2014) and are distinguished by the ability to release 1,2- and/or 1,3-linked Araf from singly or
57 doubly substituted Xylp residues (Van Laere et al. 1999; Sakamoto et al. 2013). Only GH62 contains exclusively ABFs
58 and it constitutes glycoside hydrolase clan F (GH-F) with GH43 (Lombard et al. 2014) that comprises ABF and several
59 other specificities. GH62 is predicted to be inverting similar to GH43 (Kellett et al. 1990; McKie et al. 1997; Kimura et
60 al. 2000) as was here confirmed experimentally by using NMR, which also demonstrated that *AnAbf62A-m2,3* releases
61 α -1,3-linked three times faster than α -1,2-linked Araf. Currently 17 GH62 members have been functionally
62 characterized and kinetic data are reported for nine (Poutanen 1988; Margolles-Clark et al. 1996; Ransom and Walton
63 1997; Vincent et al. 1997; Lange et al. 2006; De La Mare et al. 2013; Siguier et al. 2014; Maehara et al. 2014; Wang et
64 al. 2014; Kaur et al. 2014), while substrate specificity was determined for the remaining eight enzymes (Kellett et al.
65 1990; Kimura et al. 2000; Hashimoto et al. 2011; Sakamoto et al. 2011). The first GH62 crystal structures – five in total
66 – were published in 2014 (Siguier et al. 2014; Maehara et al. 2014; Wang et al. 2014; Kaur et al. 2014) and share a five-
67 bladed β -propeller fold catalytic domain with the six GH43 ABF structures of one fungal and five bacterial enzymes
68 (Nurizzo et al. 2002; Lombard et al. 2014). Single mutants support the role of invariant glutamic acid and aspartic acid
69 residues as general acid and base catalyst and of another invariant aspartic acid residue as pK_a modulator of the acid
70 catalyst (Pitson et al. 1996; Nurizzo et al. 2002; Siguier et al. 2014).

71 The present study concerns *AnAbf62A-m2,3*, one of the two *Aspergillus nidulans* GH62 enzymes available in the
72 seminal tool box of *Pichia pastoris* transformants encoding *A. nidulans* plant cell wall degrading enzymes (Bauer et al.
73 2006). *AnAbf62A-m2,3* has no carbohydrate binding module (CBM) therefore its strong binding to different cell wall
74 polysaccharides motivated establishing a homology model in which Trp²³ and Tyr⁴⁴ were tentatively localized to a
75 surface binding site (SBS). In the light of the number of GH62 sequences in CAZy which is very recently grown by 40
76 % we here divided GH62 in four phylogenetics subgroups (Supplementary Fig. S1) rather than just two (Siguier et al.
77 2014).

78

79 **Materials and methods**

80

81 Structural modelling and phylogenetic subgrouping

82

83 An *AnAbf62A*-m2,3 model obtained using HHpred (Söding et al. 2005) and the structure of *SthAbf62A* from
84 *Streptomyces thermoviolaceus* (PDB ID 4O8O) as template was judged as “extremely good/very good” (LGscore 5.1
85 and MaxSub 0.54) by ProQ (Wallner and Elofsson 2003). Alignment with *SthAbf62A* using PyMol 1.3 (Schrödinger,
86 LLC, New York, NY, USA; also used for rendering structural models) showed similar secondary structural elements
87 (prediction server PSIPRED (Buchan et al. 2010)) having two *AnAbf62A*-m2,3 outliers (Thr²⁰² and Asn²⁸⁷) in the
88 Ramachandran plot. The overall rmsd for C α was 0.15 Å.

89 The catalytic domain (cl14647) was identified by Conserved Domain Database (Marchler-Bauer and Lu 2011) in 142
90 GH62 sequences (May 15 2015) retrieved from CAZy and a multiple alignment (ClustalW default settings within
91 MEGA 6 (Tamura et al. 2013)) was generated for building a phylogenetic tree using the maximum likelihood algorithm
92 with MEGA 6 (Tamura et al. 2013). Peptide Pattern Recognition (Busk and Lange 2013) identified unique sequence
93 motifs for the subgroups with the following parameters (peptide length: 7; number of peptides: 70; cut-off: 10). The
94 identities were calculated by aid of ClustalW 2.1 (Li et al. 2015).

95

96 Cloning, mutagenesis, expression and purification of *AnAbf62A*-m2,3

97

98 *P. pastoris* X-33 transformants (FGSC database accession no. 10088 and 10106; www.fgsc.net) harbouring full-length
99 *A. nidulans* FGSC A4 ABF (GenBank ID: AN7908.2) were purchased (Fungal Genetics Stock Centre, School of
100 Biological Sciences, University of Missouri-Kansas City, MO, USA). A 22 residues predicted signal peptide (SignalP
101 3.0 (Emanuelsson et al. 2007)) was removed using PCR (Expand High Fidelity DNA polymerase; Roche Diagnostics,
102 Rotkreuz, Switzerland) (for primers see Supplementary Table S1) and a C2A mutation was introduced to avoid
103 intermolecular disulfide formation. The construct was cloned (using *EcoRI* and *NotI*; New England BioLabs, Ipswich,
104 MA, USA) in-frame in pPICZ α A (Invitrogen, Carlsbad, CA, USA) with the sequence for the *Saccharomyces cerevisiae*
105 α -mating factor and a stop codon upstream of a C-terminal His-tag (QuickChange kit; Stratagene, San Diego, CA, USA;
106 Supplementary Table S1). A pPICZ α A-*AnAbf62A*-m2,3 transformant (*Escherichia coli* DH5 α selected on low salt LB
107 medium with 25 μ g/ml zeocin; Novagen, Nottingham, United Kingdom) was sequenced (Eurofins MWG Operon,
108 Ebersberg, Germany), linearized (*PmeI*; New England BioLabs, Ipswich, MA, USA), transformed into *P. pastoris* X-33
109 (Micropulser; Bio-Rad, Hercules, CA, USA), and selected (30 °C, 3 d) on yeast peptone dextrose plates with 100 μ g/ml
110 zeocin (Invitrogen, Carlsbad, CA, USA). *AnAbf62A*-m2,3 W23A, D28A, Y44A, D136A, E188A, and W23A/Y44A
111 mutants were made using site-directed mutagenesis (for primers see Supplementary Table S1) according to the
112 manufacturer’s recommendations (QuickChange kit; Stratagene, San Diego, CA, USA). *P. pastoris* transformants were
113 grown in shake flasks in buffered glycerol-complex medium (BMGY; 30 °C, 24 h), harvested (3000g, 10 min, 22 °C)
114 and resuspended to 1/4 of the BMGY culture volume in buffered methanol-complex medium (BMMY; 22 °C, 96 h;
115 methanol supplemented to 0.5 % (v/v) every 24 h). Supernatants were filtered (0.45 μ m Durapore membrane filters;
116 Millipore, Billerica, MA, USA), 10 fold concentrated and buffer-exchanged to 10 mM sodium acetate pH 5.5 (Pellicon
117 ultra-filtration unit, 10 kDa cut-off filter; Millipore, Billerica, MA, USA), applied (5 ml/min) onto a 15 ml CptoQ

118 column (GE Healthcare, Little Chalfont, United Kingdom) equilibrated with 10 mM sodium acetate pH 5.5 and eluted
119 by a linear 0–500 mM NaCl gradient (20 CV) (5 ml/min). Fractions containing *AnAbf62A-m2,3* (monitored by SDS-
120 PAGE) were pooled, concentrated (4000g; Amicon Ultra-15 centrifugal filter units, 10 kDa cut-off; Millipore, Billerica,
121 MA, USA) and gel filtrated (Hiload 26/60 Superdex G75 column; GE Healthcare, Little Chalfont, United Kingdom) in
122 10 mM sodium acetate, 0.15 M NaCl, pH 5.5 (0.5 ml/min). Fractions containing *AnAbf62A-m2,3* were pooled,
123 concentrated and buffer-exchanged to 10 mM HEPES pH 7.5, applied (2 ml/min) to a 6 ml ResourceQ column (GE
124 Healthcare, Little Chalfont, United Kingdom) in this buffer and eluted by a linear 0–500 mM NaCl gradient (20 CV; 2
125 ml/min). Pure *AnAbf62A-m2,3* was pooled, concentrated (to 30–970 μ M), buffer-exchanged to 10 mM sodium acetate
126 pH 5.5, added sodium azide to 0.02 % and stored at 4 °C. All steps were carried out at 4 °C.

127

128 Protein analyses

129

130 *AnAbf62A-m2,3* wild-type and mutants were analysed by SDS-PAGE (4–12 %; Invitrogen). Molecular mass of wild-
131 type was determined by ESI-MS (LCT Premier mass spectrometer; Waters, Milford, MA, USA). Briefly, *AnAbf62A-*
132 *m2,3* was exchanged into 2.3 M ammonium acetate (Micro Bio-Spin P-6 size exclusion columns; Bio-Rad, Hercules,
133 CA, USA), sprayed from nanoES capillaries (ES380; Proxeon, Odense, Denmark) using the parameters; capillary
134 voltage: 900–1500 V; sample cone voltage: 25 V; source temperature: 30 °C; and cone gas flow: 20 L/h (N₂) and
135 spectra were collected in positive ion mode. The instrument was calibrated with 100 mg/ml CsI in 50 % (v/v)
136 isopropanol. Spectra were processed by smoothing followed by manual deconvolution (MassLynx V4.1 software;
137 Waters, Milford, MA, USA). Protein concentration was determined by aid of amino acid analysis (Barkholt and Jensen
138 1989). The melting temperature (T_m) was determined by far-UV CD spectroscopy (see [Supplementary Fig. S2](#)).
139 Deglycosylation by endoglycosidase H was attempted under native and denaturing conditions as recommended by the
140 manufacturer (New England Biolabs, Ipswich, MA, USA).

141

142 Affinity gel electrophoresis

143

144 *AnAbf62A-m2,3* and mutants (4 μ g in sample buffer, 0.25 M Tris base, 0.12 M boric acid, 40 % glycerol, 0.05 %
145 Bromphenol Blue, pH 8.7) were applied on 12 % (w/v) polyacrylamide gel cast with 0.001–1 % (w/v) low viscosity
146 wheat AX (WAX-LV) (Megazyme, Wicklow, Ireland), oat spelt xylan, birchwood xylan (both Carl Roth, Karlsruhe,
147 Germany), larch arabinogalactan, sugar beet L-arabinan (both Megazyme, Wicklow, Ireland), acacia tree gum arabic,
148 hydroxyethyl cellulose (both Sigma-Aldrich, St. Louis, MI, USA), or barley β -glucan (Novo Industries, Gentofte,
149 Denmark), and run in 0.25 M Tris base, 0.12 M boric acid, pH 8.7 (4 °C, 50 V, 16 h, XCell SureLock[®] Mini-Cell
150 system; Invitrogen, Carlsbad, CA, USA) with reference proteins (NativeMark; Invitrogen, Carlsbad, CA, USA) in the
151 same tank as a control without polysaccharide. Proteins were visualized by Simpleblue SafeStain (Invitrogen, Carlsbad,
152 CA, USA). WAX-LV was dissolved in water (50 °C) and kept for 1 h. Birchwood and oat spelt xylans were dissolved
153 in water in a microwave oven, and sugar beet L-arabinan, acacia tree gum arabic, and larch arabinogalactan in water
154 (RT). Barley β -glucan was wet with a minimum volume 95 % ethanol, suspended in cold water with stirring, heated to

155 boiling with stirring and stirred for 1 h. Hydroxyethyl cellulose was dissolved in 10 mM sodium phosphate pH 6 and
156 adjusted to pH 8.

157 The relative retardation of migration (R_m) by the polysaccharide compared to the control was determined from the
158 following equation: $R_m = R_{mi} / R_{mo}$, where R_{mi} and R_{mo} are migration distances of sample relative to reference protein in
159 the presence and in the absence of polysaccharide, respectively.

160

161 Enzyme activity assays

162

163 *4NP-glycosides*: 10 mM 4NPaf, 4-nitrophenyl- β -D-xylopyranoside (4NPX) (Sigma-Aldrich, St. Louis, MI, USA) or 4-
164 nitrophenyl- α -L-arabinopyranoside (4NPap) (Sigma-Aldrich, St. Louis, MI, USA) in water (20 μ l) was preincubated
165 with 125 mM sodium acetate, 0.005 % Triton-X-100, pH 5.5 (20 μ l; 2 min; 37°C) and added *AnAbf62A-m2,3* (10 μ l;
166 12–24 μ M final concentration). The reaction (10 min; 37 °C) was stopped by 1 M Na_2CO_3 (200 μ l) and 4NP quantified
167 spectrophotometrically at 410 nm (200 μ l; microtiter plate reader; Bio-Tek Instrument Inc., Winooski, VT, USA) using
168 4NP (0–0.5 mM) as standard. One activity unit (U) was defined as the amount of enzyme releasing 1 μ mol/min 4NP.
169 Kinetic parameters were determined from initial rates of 4NPaf (0.05–4 mM) hydrolysis by *AnAbf62A-m2,3* (0.25–0.5
170 μ M; monitored up to 16 min). pH activity optimum was determined using 2.5 mM 4NPaf in 40 mM Britton-Robinson
171 universal buffers pH 2–10 (Britton and Robinson 1931) and 50 mM sodium acetate pH 5.0–6.0 (37 °C). The
172 temperature optimum was determined at pH 5.5 for 25–75 °C.

173 *Polysaccharides*: Activity was tested on 0.9 % (w/v) linear L-arabinan (Megazyme Wicklow, Ireland), birchwood
174 xylan, and barley β -glucan in 50 mM sodium acetate, 0.005 % Triton X-100 pH 5.5 incubated (30 min; 37 °C) with 97
175 μ M *AnAbf62A-m2,3* and quantifying reducing sugar by adding 3,5-dinitrosalicylic acid reagent (600 μ l; 1 % DNS, 0.2
176 % phenol, 0.05 % NaSO_3 , 1 % NaOH, and 20 % NaK-tartrate), heated (95 °C; 15 min), cooled (on ice; 15 min) and
177 measuring A_{540} (Mohun and Cook 1962) (200 μ l; microtiter plate reader) using L-arabinose as standard. Specific
178 activity for 0.9 % WAX-LV, rye AX (Megazyme, Wicklow, Ireland), oat spelt xylan, larch arabinogalactan, sugar beet
179 L-arabinan, and acacia tree gum arabic was determined for 0.05 μ M *AnAbf62A-m2,3* in the above buffer (10 min
180 reaction) and L-arabinose quantified by the lactose/D-galactose (rapid) kit (Megazyme, Wicklow, Ireland) (see below).
181 One activity unit (U) was defined as the amount of enzyme releasing 1 μ mol/min arabinose. The effect on hydrolysis of
182 0.1 % WAX-LV and 0.4 mM or 6 mM 4NPaf by barley β -glucan or birchwood xylan (0.05–0.8 %; 0.1 % with 4NPaf)
183 was measured assaying released L-arabinose by the lactose/D-galactose kit (see below).

184 Kinetic parameters were determined from initial rates of L-arabinose release (lactose/D-galactose (rapid) kit
185 (Megazyme, Wicklow, Ireland)) from WAX-LV (0.28–9 mg/ml) and sugar beet L-arabinan (4–90 mg/ml) in the above
186 buffer (37 °C). Reactions were initiated by adding enzyme (WAX-LV: 0.03–2 μ M; sugar beet L-arabinan: 1–5 μ M).
187 Aliquots (50 μ l) were removed during 16 min (60 min for catalytic site mutants), added to 1 M Tris-HCl pH 8.6 (200
188 μ l) followed by incubation (40 min; RT) with lactose/D-galactose kit solution (880 μ l) and quantified (200 μ l; microtiter
189 plate reader; $\text{NADH } \epsilon_{M,340} = 6300 \text{ M}^{-1} \times \text{cm}^{-1}$) using L-arabinose (0–1.75 mM) as standard. k_{cat} , K_m , and K_i were obtained
190 (SigmaPlot 9.01; SYSTAT software Inc., San Jose, CA, USA) by fitting either the classical Michaelis Menten $V = V_{max}$
191 / (1 + (K_m / [S]) or the modified equation including a term for uncompetitive substrate inhibition $V_{i,s} = V_{max} / (1 + ((K_m /$
192 [S]) + ([S] / $K_i))$ to initial rate data. V and $V_{i,s}$ are reaction rates, V_{max} maximum rate, [S] substrate concentration, and K_i

193 dissociation constant for inhibited ternary [substrate-enzyme]-substrate complex. Catalytic efficiency (k_{cat}/K_m) is
194 reported for 4NPAf, as K_m is too high to be determined.

195 Specificity analysis was also done by polysaccharide analysis by carbohydrate gel electrophoresis (PACE) as described
196 (Goubet et al. 2002) and visualised according to (Bromley et al. 2013). For PACE, WAX was treated with *NpXyn11A*
197 (Vardakou et al. 2008), *HiAbf43* (McKee et al. 2012) and *AnAbf62A-m2,3* to generate the xylooligosaccharides and
198 AXOS labelled and used to analyse the specificity of *AnAbf62A-m2,3* essentially as described (McKee et al. 2012).

199 AXOS: Specific activity of *AnAbf62A-m2,3* (final concentration: 0.5 μ M) was analysed on 53.7 mM (final
200 concentration) A^3X [α -L-Araf-(1 \rightarrow 3)- β -D-Xylp-(1 \rightarrow 4)-D-Xylp], 40.7 mM A^2XX [α -L-Araf-(1 \rightarrow 2)- β -D-Xylp-(1 \rightarrow
201 4)- β -D-Xylp-(1 \rightarrow 4)-D- β -Xylp], a mixture of 40.7 mM (final concentration) A^2XX [α -L-Araf-(1 \rightarrow 2)- β -D-Xylp-(1 \rightarrow
202 4)- β -D-Xylp-(1 \rightarrow 4)-D- β -Xylp] (70 %) plus A^3XX [α -L-Araf-(1 \rightarrow 3)- β -D-Xylp-(1 \rightarrow 4)- β -D-Xylp-(1 \rightarrow 4)-D- β -
203 Xylp] (30 %), a mixture of 32.8 mM (final concentration) XA^3XX [β -D-Xylp-(α -L-Araf-(1 \rightarrow 3)- β -D-Xylp-(1 \rightarrow 4)- β -
204 -D-Xylp-(1 \rightarrow 4)- β -D-Xylp (50%) plus XA^2XX [β -D-Xylp-(1 \rightarrow 4)-[α -L-Araf-(1 \rightarrow 2)]- β -D-Xylp-(1 \rightarrow 4)- β -D-Xylp]
205 (50%), and 32.8 mM (final concentration) $A^{2+3}XX$ [α -L-Araf-(1 \rightarrow 2)]-[α -L-Araf-(1 \rightarrow 3)]- β -D-Xylp-(1 \rightarrow 4)- β -D-
206 Xylp-(1 \rightarrow 4)- β -D-Xylp] prepared in 33 mM sodium acetate pH 4.5 at 40 °C and released L-arabinose was quantified
207 using the lactose/D-galactose kit as described previously (McCleary et al. 2015).

208 Relative activities of wild-type (3.7 μ M), W23A (4.4 μ M), Y44A (3.3 μ M) and W23A/Y44A (11 μ M) were analysed as
209 above using 2.5 mM AX^3 , XA^2XX+XA^3XX and A^2XX [α -L-Araf-(1 \rightarrow 2)- β -D-Xylp-(1 \rightarrow 4)- β -D-Xylp-(1 \rightarrow 4)-D- β -
210 Xylp] (69.5 %), XA^3X [β -D-Xylp-(1 \rightarrow 4)-[α -L-Araf-(1 \rightarrow 3)]- β -D-Xylp-(1 \rightarrow 4)- β -D-Xylp] (19 %) plus A^3XX [α -L-
211 Araf-(1 \rightarrow 3)- β -D-Xylp-(1 \rightarrow 4)- β -D-Xylp-(1 \rightarrow 4)- β -D-Xylp] (11.5 %) (Barry McCleary, in house collection).

212 Action pattern towards α -1,2- and α -1,3-Araf decorated Xylp and the stereochemical course were both determined by
213 NMR. Hydrolysis of 1 mg/ml of XA^3XX+XA^2XX by *AnAbf62A-m2,3* (0.03 nM), $A^{2+3}X$ [[α -L-Araf-(1 \rightarrow 2)]-[α -L-
214 Araf-(1 \rightarrow 3)]- β -D-Xylp-(1 \rightarrow 4)- β -D-Xylp] (by 0.25 μ M *AnAbf62A-m2,3*), and $A^{2+3}XX$ [[α -L-Araf-(1 \rightarrow 2)]-[α -L-
215 Araf-(1 \rightarrow 3)]- β -D-Xylp-(1 \rightarrow 4)- β -D-Xylp-(1 \rightarrow 4)- β -D-Xylp] (by 0.25 μ M *AnAbf62A-m2,3*) in 10 mM sodium
216 phosphate pH 6 was monitored (800 MHz Bruker Avance II NMR spectrometer equipped with a TCI cryoprobe;
217 Bruker, Billerica, MA, USA) at 308 K and referenced relative to acetone ($\delta^1H=2.225$ ppm; $\delta^{13}C=30.89$ ppm). $A^{2+3}X$
218 and $A^{2+3}XX$ are kind gifts of Maija Tenkanen. For kinetic experiments a series of 1D proton spectra were recorded and
219 for assignment a series of homo- and heteronuclear 2D spectra were recorded as DQF-COSY, NOESY with 600 ms
220 mixing time, TOCSY with a spin lock field applied for 60 ms, a multiplicity edited 1H - ^{13}C HSQC and a 1H - ^{13}C HMBC.
221 The stereochemical course of XA^2XX+XA^3XX hydrolysis was followed at 308 K by 1H NMR with single scan 1D
222 proton experiments of 11.5 s intervals. The first spectrum was recorded 23 s after enzyme addition.

223

224 Results

225

226 GH62 phylogenetic subgrouping

227

228 Phylogenetic analysis combined with a peptide pattern search using PPR (Busk and Lange 2013) of 142 GH62
229 sequences revealed four distinct subfamilies (Supplementary Fig. S1). GH62_2, the largest subfamily, contains 103 55–

230 100 % identical amino acid sequences and corresponds to the GH62_2 subfamily defined previously (Siguier et al.
231 2014). GH62_1 has 25 39–100 % identical sequences, GH62_3 and GH62_4 each have seven 29–100 % and 57–85 %
232 identical sequences, respectively. *AnAbf62A*-m2,3 belongs to subfamily GH62_2 (Supplementary Fig. S1). It remains
233 to be uncovered if these subfamilies and the assigned unique sequence motifs (Supplementary Fig. S3) represent distinct
234 enzymatic properties. Enzyme kinetics is reported for two GH62_1 (Couturier et al. 2011; Siguier et al. 2014; Kaur et
235 al. 2014) and 12 GH62_2 members (Poutanen 1988; Vincent et al. 1997; Kimura et al. 2000; Tsujibo et al. 2002;
236 Sakamoto et al. 2011; Hashimoto et al. 2011; De La Mare et al. 2013; Siguier et al. 2014; Maehara et al. 2014; Wang et
237 al. 2014; Kaur et al. 2014; McCleary et al. 2015), whereas no GH62_3 member has been characterised and one from
238 GH62_4 was shown to degrade oat spelt xylan (Kellett et al. 1990).

239

240 Structural model

241

242 The model of *AnAbf62A*-m2,3 generated based on *SthAbf62A* from *S. thermoviolaceus* (PDB ID 4O8O) of 73 %
243 sequence identity (Wang et al. 2014) showed a five-bladed β -propeller fold domain. Overlays of arabinose and
244 xylopentaose from structures of *SthAbf62A* (PDB ID 4O8O) and *Streptomyces coelicolor* *ScAf62A* (PDB ID 3WN2)
245 (Maehara et al. 2014) complexes (Fig. 1) indicated possible substrate interactions in *AnAbf62A*-m2,3 to involve at least
246 three main chain binding subsites towards the non-reducing end (+2NR, +3NR, +4NR), one subsite towards the
247 reducing end (+2R) and subsites –1 and +1 accommodating *Araf* to be cleaved off and the *Xylp* it decorates,
248 respectively. Equivalent residues at these subsites in *AnAbf62A*-m2,3 and the five GH62 crystal structures are shown
249 (Fig. 2).

250

251 Purification and physico-chemical characterization

252

253 *AnAbf62A*-m2,3 wild-type, three mutants at the catalytic site and three at the putative SBS were obtained in yields of
254 150–235 mg/l from *P. pastoris* culture supernatants and migrated in SDS-PAGE as two close bands of apparent
255 molecular weights 34 and 36 kDa (Supplementary Fig. S4). ESI-MS of *AnAbf62A*-m2,3 wild-type gave M_r of 33327.3
256 \pm 0.3 and 33633 \pm 1 differing by 306 for the lower band, while for the upper and minor band five M_r values in the range
257 35434–36067 differed by approximately 162 corresponding to one hexose residue. Mass deviations of 139 Da and
258 2.4–2.8 kDa from the theoretical M_r of 33188.5, presumably reflect misprocessing of the signal peptide and / or *O*-
259 glycosylation, which was not eliminated by endoglycosidase H treatment. *AnAbf62A*-m2,3 forms corresponding to
260 either of the 34 and 36 kDa bands, were purified in extremely low yield (<1%) by gel filtration (Supplementary Fig.
261 S5), and found to have the same specific activity towards WAX, therefore *AnAbf62A*-m2,3 wild-type and mutants were
262 characterised without being subjected to this inefficient purification of each form. The conformational stability of wild-
263 type and mutants was assessed by aid of CD spectroscopy and T_m values were determined to 71.53 \pm 0.28 $^{\circ}$ C (wild-
264 type), 69.96 \pm 0.19 (D28A), 70.11 \pm 0.20 (E188A), 62.48 \pm 0.18 (D136A), 60.83 \pm 0.22 (W23A), 64.63 \pm 0.20 (Y44A),
265 and 55.41 \pm 0.49 (W23A/Y44A) (Supplementary Fig. S2A–G).

266

267 Affinity for polysaccharides

268

269 *AnAbf62A*-m2,3 interacted exceptionally strongly with 0.05 % WAX-LV in AE (Fig. 3A) and got still importantly
270 retarded by 0.001 % WAX-LV ($R_m=0.67$) (Fig. 3C; Supplementary Table S2), oat spelt xylan ($R_m=0.73$) (Fig. 3D;
271 Supplementary Table S2) or birchwood xylan ($R_m=0.80$) (Fig. 3E; Supplementary Table S2). *AnAbf62A*-m2,3 thus
272 recognises the xylan backbone as birchwood xylan has very few (< 1%) or no *Araf* substituents (Kormelink and
273 Voragen 1993; Li et al. 2000). Two closely migrating bands of the *AnAbf62A*-m2,3 control (Fig. 3B) merged in AE
274 indicating all *AnAbf62A*-m2,3 forms bind polysaccharides. By contrast 1 % sugar beet L-arabinan ($R_m=1$) (Fig. 3G;
275 Supplementary Table S2), acacia tree gum Arabic ($R_m=1$) (Fig. 3H), or larch arabinogalactan ($R_m=1$) (Fig. 3I;
276 Supplementary Table S2) did not retard the enzyme in AE even though they are decorated by *Araf* and L-arabinan is a
277 substrate (Table 1). Notably, *AnAbf62A*-m2,3 contains no CBM but clearly binds to 0.001 % barley β -glucan ($R_m=0.9$)
278 (Fig. 3F; Supplementary Table S2) and hydroxyethyl cellulose (not shown), which are not substrates. This affinity for
279 β -glucans may be reminiscent to the accommodation of cellotriose at the active site in the *PaAbf62A* structure (Siguier
280 et al. 2014).

281

282 Substrate specificity and mechanism of action

283

284 *AnAbf62A*-m2,3 degraded WAX-LV with exceptional high activity of 67.42 U/mg (Table 1), $k_{cat} = 178 \text{ s}^{-1}$ and $K_m = 2.3$
285 mg/ml (Table 2, Fig. 4A). WAX-LV exerted uncompetitive substrate inhibition with $K_i = 2.89 \text{ mg/ml}$ (Table 2, Fig. 4A)
286 and inhibited hydrolysis of 4NPAf by ~60 % (data not shown). *AnAbf62A*-m2,3 has almost the same high activity on
287 rye AX and oat spelt xylan (Table 1), but low activity without substrate inhibition for sugar beet L-arabinan of $k_{cat} =$
288 1.03 s^{-1} and $K_m = 15.63 \text{ mg/ml}$ (Table 2, Fig. 4A, B). *Araf* substituted larch arabinogalactan and acacia tree gum arabic
289 were extremely poor substrates and unsubstituted sugar beet linear arabinan was not degraded (Table 1). Birchwood
290 xylan and barley β -glucan were neither substrates of *AnAbf62A*-m2,3 nor inhibited its hydrolysis of WAX-LV and
291 4NPAf. *AnAbf62A*-m2,3 showed moderate activity with 4NPAf and optimum at pH 5.5 and 50 °C (Table 1;
292 Supplementary Fig. S6A–C); its activity towards 4NPAP and 4NPX was 2–3 % compared to 4NPAf (Table 1).

293 ^1H NMR analyses demonstrated that *AnAbf62A*-m2,3 hydrolysed 1,2- and 1,3-*Araf* in $\text{XA}^2\text{XX}+\text{XA}^3\text{XX}$ (1:1) in singly,
294 but not from 1,2- / 1,3-*Araf* doubly substituted *Xylp* in XA^{2+3}X and XA^{2+3}XX and 1,3- was released three times faster
295 than 1,2-linked *Araf* (Table 1, Fig. 5, Supplementary Figs. S7 and S8). Additionally, ^1H -NMR showed that *AnAbf62A*-
296 m2,3 liberated β -furanose (assigned anomer resonance: 5.283 ppm) from $\text{XA}^2\text{XX}+\text{XA}^3\text{XX}$ (Fig. 5, Supplementary Fig.
297 S7). Due to fast mutarotation, however, the anomeric signal decreased considerably already after 1 min (Fig. 5,
298 Supplementary Fig. S7). The same specificity was determined by PACE using AXOS and WAX as substrates
299 (Supplementary Fig. S9). *AnAbf62A*-m2,3 attacked A^3XX and XA^2XX , but not the doubly 1,2- / 1,3-*Araf* substituted
300 *Xylp* in XA^{2+3}XX . Hydrolysis of WAX by *AnAbf62A*-m2,3 followed by *NpXyn11A*, predominantly released
301 XA^{2+3}XX , xylobiose, xylose and arabinose, confirming the specificity of *AnAbf62A*-m2,3 on the polysaccharide.

302 Finally, alanine mutants of the invariant catalytic site Asp²⁸, Glu¹⁸⁸ and Asp¹³⁶ retained 7.7×10^{-3} , 5.9×10^{-4} and 6.1×10^{-3}
303 fold of wild-type activity for WAX-LV (Table 2, Fig. 4C). While D28A showed Michaelis-Menten kinetics on WAX-
304 LV, D136A complied with the uncompetitive substrate inhibition found for wild-type, but K_i was doubled (Table 2, Fig.
305 4C). The activity of the general acid E188A mutant was too low for kinetic analysis. The results agreed with the roles in

306 catalysis of the three residues as general base, general acid catalysts and acid catalyst pK_a modulator, respectively, also
307 supported by crystal structures of *UmAbf62A*, *PaAbf62A* (Siguier et al. 2014) and *ScAraf62A* (Maehara et al. 2014).

308

309 Interaction at a putative surface binding site

310

311 In the structural model of *AnAbf62A*-m2,3 Trp²³ and Tyr⁴⁴ are situated near the active site cleft, at a distance of about
312 30 Å from the catalytic site in a shallow cleft that runs perpendicular to the active site cleft, and which is almost a
313 continuation of this (Fig. 1; 6A, B; Supplementary 3D data). Trp²³ is conserved in 71 % of the 142 GH62 sequences,
314 which all belong to GH62_2 and six of seven GH62_3 sequences. Tyr⁴⁴ is seen in 10 (7 %) GH62_2 sequences and all
315 10 have Trp²³. The interaction in AE with WAX-LV, oat spelt xylan, birchwood xylan and barley β -glucan clearly
316 weakened for W23A and W23A/Y44A, but not for the Y44A mutant that displayed essentially wild-type retardation
317 (Fig. 3C–E; Supplementary Table S2). While W23A/Y44A retained some binding with the AXs and birchwood xylan
318 in AE, this is not the case for barley β -glucan (Fig. 3C–F; Supplementary Table S2). Thus substitution of two aromatic
319 residues at a putative surface binding site (SBS) situated outside of the active site cleft differentially affected
320 polysaccharide binding specificity of *AnAbf62A*-m2,3.

321 Mutation of Trp²³ and Tyr⁴⁴ did not dramatically alter k_{cat} and K_m for WAX-LV, sugar beet L-arabinan and 4NPAf
322 (Table 2, Fig. 4A, D). Remarkably, however, K_i of WAX-LV substrate inhibition increased 4–7 fold for the three
323 mutants relative to wild-type (Fig. 4D, Table 2) suggesting significant AX interaction involving Trp²³ and Tyr⁴⁴ to be
324 clearly diminished in the mutants accompanied by modest effect on activity (Table 2, Fig. 3A), which can be interpreted
325 as an effect of lack of or reduced affinity for WAX at the SBS. Remarkably, depending on the mutant and size of
326 AXOS (Table 3) only 4–23 % activity was the retained even though Trp²³ and Tyr⁴⁴ according to the *AnAbf62A*-m2,3
327 model (Figs. 1 and 6) are not situated at subsites accommodating AXOS for productive binding.

328

329 Discussion

330

331 Knowledge on GH62s is important to provide guidance on ABFs best suited for specific applications. For example
332 addition of *AnAbf62A*-m2,3 to unhydrolysed oligosaccharides from switchgrass treated with commercial enzymes
333 efficiently improved the extent of conversion (Bowman et al. 2015). While insights on structure, substrate specificity,
334 and mechanism of action in a broader sense are gained from sequence based classification of ABFs into GH families
335 (Lombard et al. 2014), understanding of substrate specificity details and linking of functional diversity with
336 phylogenetics require experimental studies. Comparison of *A. nidulans AnAbf62A*-m2,3 with other GH62 enzymes
337 underscored its unusually high activity on both AXs and AXOS and disclosed a putative SBS implicated in activity and
338 interaction with cell wall polysaccharides.

339

340 Activity and structure/function relationships

341

342 *AnAbf62A*-m2,3 cleaves off 1,2- and 1,3-Araf from mono-substituted Xylp in AXOS and AX and the same specificity
343 was reported for other GH62_2 members *SthAbf62A* (Wang et al. 2014), *StAbf62A* (Kaur et al. 2014), *Penicillium*
344 *chrysogenum* AXS5 (Sakamoto et al. 2011), *Penicillium funiculosum* ABF62a–c (De La Mare et al. 2013), *Penicillium*

345 *capsulatum* ABF (Lange et al. 2006), and *StAbf62C* of GH62_1 (Kaur et al. 2014). The rate of release analysed by ¹H
346 NMR was three times faster for 1,3- than 1,2-*Araf* probably reflecting that 1,3- and 1,2-linked *Araf* residues bind
347 productively in opposite directions (Maehara et al. 2014; Wang et al. 2014).

348 *AnAbf62A-m2,3* acts on WAX-LV with 67.42 compared to 0.15–13 U/mg reported for 13 other GH62s (Kellett et al.
349 1990; Vincent et al. 1997; Kimura et al. 2000; Hashimoto et al. 2011; Sakamoto et al. 2011; Couturier et al. 2011; De
350 La Mare et al. 2013; Siguier et al. 2014; Maehara et al. 2014; Kaur et al. 2014). *S. thermoviolaceus StAbf62A*,
351 however, shows ~30 U/mg with WAX-HV (HV = high viscosity) of *Araf:Xylp* ratio of 0.5, which is a superior substrate
352 to WAX-LV with *Araf:Xylp* of 0.3 (Pitkänen et al. 2009) on which *StAbf62A* shows ~18 U/mg (Wang et al. 2014).
353 *AnAbf62A-m2,3* has k_{cat} of 178 s⁻¹ on WAX-LV (Table 2, Fig. 4A) compared to k_{cat} = 180 s⁻¹ of *StAbf62A* determined
354 with the superior substrate, WAX-HV (Wang et al. 2014). Other GH62s gave much lower k_{cat} of 0.3–1.5 s⁻¹ against
355 WAX-LV and WAX-HV (Vincent et al. 1997; De La Mare et al. 2013; Siguier et al. 2014; Maehara et al. 2014; Kaur et
356 al. 2014). K_m of *AnAbf62A-m2,3* is 2.3 mg/ml for WAX-LV (Table 2, Fig. 4A), which is intermediate to K_m values of 1
357 mg/ml for *AbfB* from *Streptomyces lividans* (Vincent et al. 1997), *ABF62b* and *ABF62c* from *P. funiculosum* (De La
358 Mare et al. 2013) and 7–12 mg/ml for *StAbf62A* from *S. thermophilum* (Wang et al. 2014), *ScAraf62A* from *S.*
359 *coelicolor* (Maehara et al. 2014) and *ABF62a* from *P. funiculosum* (De La Mare et al. 2013). *S. lividans AbfB* contains
360 a putative CBM, for which the specificity has not been tested without the catalytic domain and it is possible therefore
361 that the binding of xylan stems from the CBM but it cannot be excluded that the interaction is with the catalytic domain
362 (Vincent et al. 1997). *ABF62c* from *P. funiculosum* has a cellulose binding CBM13 (De La Mare et al. 2013) perhaps
363 contributing to substrate binding, while *StAbf62A* has a cellulose binding CBM1 (Wang et al. 2014). *S. thermophilum*
364 *StAbf62C* has K_m = 3.7 mg/ml (Kaur et al. 2014) which is similar to *AnAbf62A-m2,3* having K_m = 4.9 mg/ml (Table 2).
365 *AnAbf62A-m2,3* and *StAbf62A* are subject to substrate inhibition with K_i of 2.89 (Table 2, Fig. 4A) and 1.5 mg/ml for
366 WAX-LV and WAX-HV (Wang et al. 2014), respectively.

367 *AnAbf62A-m2,3* is slightly more active on oat spelt xylan and rye AX than *StAbf62A* (Wang et al. 2014) and neither
368 *AnAbf62A-m2,3* nor five other GH62s degraded birchwood xylan (Vincent et al. 1997; Tsujibo et al. 2002; Hashimoto
369 et al. 2011; Sakamoto et al. 2011; Wang et al. 2014).

370 GH62s differ conspicuously in activity level for sugar beet L-arabinan and *AnAbf62A-m2,3* thus has 173- and 3-fold
371 lower and higher k_{cat} and K_m , respectively, than on WAX-LV (Table 2, Fig. 4A,B), whereas *PaAbf62A* and *UmAbf62A*
372 have k_{cat} 3- and 8-fold higher than *AnAbf62A-m2,3* for sugar beet L-arabinan, but these k_{cat} values were similar to and
373 only 3-fold higher, respectively, compared to their values obtained with WAX-LV (Siguier et al. 2014). *StAbf62A*,
374 however, has a 30-fold lower k_{cat} of 6 s⁻¹ for L-arabinan than WAX-HV. The ability to accommodate both AX and
375 arabinan was reported to involve structural movements upon binding of the xylan main chain in *StAbf62A* (Wang et
376 al. 2014). *AnAbf62A-m2,3* has 3–4 orders of magnitude lower activity for *Araf* substituted larch arabinogalactan and
377 acacia tree gum arabic than WAX (Table 1) and did not hydrolyse unsubstituted linear sugar beet arabinan. As for other
378 GH62s α -L-1,5 linked *Araf* was not a substrate (Vincent et al. 1997; Tsujibo et al. 2002; Hashimoto et al. 2011; De La
379 Mare et al. 2013; Kaur et al. 2014). *ScAraf62A* was unable to accommodate L-arabinan at the active site as deduced
380 both from lack of activity and the crystal structure (Maehara et al. 2014). Apparently substrate interactions differ
381 between *AnAbf62A-m2,3* and *ScAraf62A* although comparison of the *AnAbf62A-m2,3* model and the *ScAraf62A*
382 structure did not reveal striking dissimilarities anticipated to result in different ability to act on arabinan. Overall we
383 conclude that the GH62 family presents important quantitative, but little qualitative variation in substrate specificity.

384

385 Catalytic mechanism

386

387 The present study provides experimental evidence for GH62 of its expected inverting mechanism by the release of β -
388 furanose from AXOS as monitored by ^1H NMR, which is in accordance with the known inverting mechanism for GH43
389 (Pitson et al. 1996) constituting clan GH-F with GH62 (Lombard et al. 2014). The very low residual activities for
390 WAX-LV of catalytic site mutants D28A (general base); E188A (general acid); and D136A ($\text{p}K_a$ modulator of the acid
391 catalyst) confirmed their proposed roles in catalysis. In comparison *StAbf62C* and *ScAraf62A* catalytic acid and base
392 mutants lost activity completely against WAX-LV and 4NPaf (Maehara et al. 2014; Kaur et al. 2014), as did
393 *SthAbf62A*, for which, however, a mutant of the acid catalyst $\text{p}K_a$ modulator retained 2.1×10^{-5} fold of wild-type activity
394 (Wang et al. 2014). A stabilising effect of the $\text{p}K_a$ modulator on the catalytic site previously proposed in case of GH43
395 (Nurizzo et al. 2002) may be reflected in the 9°C loss in T_m of *AnAbf62A*-m2,3 D136A (Supplementary Fig. S2E, H).

396

397 Possible importance of the non-reducing and reducing end subsites

398

399 At subsites +2R, +1, +1NR, +2NR and +3NR in GH62 structures the residues vary and no hint to the higher activity of
400 *AnAbf62A*-m2,3 and *SthAbf62A* towards WAX can be deduced from the structures (Fig. 2). At subsite -1 both
401 *AnAbf62A*-m2,3 and *SthAbf62A* have tryptophan and threonine that interact with the Araf (Trp^{51} and Thr^{43} , *AnAbf62A*-
402 m2,3 numbering), whereas the other enzymes have tyrosine and threonine, respectively (Fig. 2). Because the two former
403 enzymes *AnAbf62A*-m2,3 and *SthAbf62A* have higher activity for WAX than reported for any other GH62 member, we
404 speculate that tryptophan at subsite -1 may be associated with their unusually high activity.

405 The level of activity of *AnAbf62A*-m2,3 was 22–48-fold higher for different AXOS than for 4NPaf suggesting that
406 subsites beyond -1 and +1 are important for a perpendicular orientation of the Xylp ring at subsite +1 positioning Araf
407 into the subsite -1 pocket (Fig. 2) (Maehara et al. 2014) and offer extra backing for productive accommodation of Araf.
408 Furthermore, two-fold higher specific activity for $\text{A}^2\text{XX}+\text{A}^3\text{XX}$ (7:3) and $\text{XA}^2\text{XX}+\text{XA}^3\text{XX}$ (1:1) compared to A^3X
409 possibly reflects importance of subsite +3NR in productive substrate binding.

410

411 Putative surface binding site

412

413 The substrate inhibition by WAX involved Trp^{23} and Tyr^{44} as the corresponding alanine mutants were less inhibited by
414 WAX and also showed improved productive binding (Table 2, Fig. 3A). Thus harmful strain or adverse binding in the
415 productive complex of WAX-LV and wild-type *AnAbf62A*-m2,3 is relieved by these mutations (Table 2, Fig. 4A).
416 Although modest changes in k_{cat}/K_m (65–104%) for 4NPaf supports retained functional integrity of subsites -1 and +1
417 remarkably, the activity of W23A, Y44A and W23A/Y44A *AnAbf62A*-m2,3 for different AXOS was only 4–23 % of
418 wild-type (Table 3), A^3X of DP3 being most affected. Activity improved with DP of both 4 ($\text{A}^2\text{XX}+\text{XA}^3\text{X}+\text{A}^3\text{XX}$) and
419 5 ($\text{XA}^2\text{XX}+\text{XA}^3\text{XX}$). Apparently occupation also of subsites towards the non-reducing end is needed for effective
420 productive AXOS interaction (Table 2), altogether suggesting that interaction with distal subsites is significant, as
421 demonstrated for *StAbf62C* by mutational analysis (Kaur et al. 2014). It may be speculated that carbohydrate binding

422 e.g. by AXOS at a secondary site in *AnAbf62A*-m2,3 involving Trp²³ and Tyr⁴⁴ allosterically triggers stimulation of
423 catalysis as known for SBSs in barley α -amylase (Oudjeriouat et al. 2003; Nielsen et al. 2012) and *Aspergillus niger*
424 xylanase (Cuyvers et al. 2011). It is likely that 4NPAf is unable to bind at or has low affinity for the SBS and the
425 W23A, Y44A and W23A/Y44A mutations therefore do not affect activity towards this substrate. As birchwood xylan
426 and barley β -glucan interact with *AnAbf62A*-m2,3, but are neither hydrolyzed nor inhibiting activity against WAX, we
427 propose a polysaccharide binding mode exists distinct from the AX substrate complex and involves an SBS containing
428 Trp²³ and Tyr⁴⁴ situated at a distance of the active site region. This is in agreement with the weakened substrate
429 inhibition by WAX-LV for the three SBS mutants, and especially the weakened interaction for W23A/Y44A leads us to
430 suggest that the SBS provides prominent interaction with the polysaccharide in conjunction with the active site.
431 In conclusion, *AnAbf62A*-m2,3 is the most active WAX-LV and AXOS degrading GH62 member reported to date. AE
432 showed *AnAbf62A*-m2,3 interacts with the Araf decorated WAX-LV and oat spelt xylan as well as birchwood xylan
433 and barley β -glucan. In conjunction with mutations of aromatic residues situated ~30 Å from the catalytic site as
434 guided by a structural model of *AnAbf62A*-m2,3, activity on AXs and AXOS suggests this site is important, whether it
435 constitutes an SBS or formally would be considered is a distal subsite. Important SBSs are recognised in certain xylan-
436 degrading enzymes in which the SBSs form shallow clefts that are almost perpendicular to the active site cleft, and most
437 often have a pair of aromatic residues located in the centre of the SBS cleft (Schmidt et al. 1999; De Vos et al. 2006;
438 Ludwiczek et al. 2007; Vandermarliere et al. 2008). Trp²³ and Tyr⁴⁴ in the *AnAbf62A*-m2,3 model are also located in a
439 shallow cleft perpendicular to the active site (Fig. 6 and Supplementary 3D data), but in the xylanases the SBSs are
440 typically found on the other side of the enzyme than the active site (Schmidt et al. 1999; De Vos et al. 2006; Ludwiczek
441 et al. 2007; Vandermarliere et al. 2008) as opposed to *AnAbf62A*-m2,3 where the shallow SBS cleft is almost a
442 continuation of the active site cleft.
443 PACE and NMR specificity analysis showed that singly substituting α -1,2- and α -1,3-linked arabinofuranose residues
444 in WAX-LV and AXOS are hydrolysed by *AnAbf62A*-m2,3. The NMR experiments confirmed release of the β -
445 arabinofuranose anomer in agreement with the inverting mechanism known for GH43 that forms GH clan-H with
446 GH62, and further demonstrated that α -1,3- is released faster than α -1,2-linked arabinofuranose residues from AXOS.

447

448 **Acknowledgements**

449

450 Mette Pries is thanked for technical assistance and Anne Blicher for amino acid analysis. The 800 MHz NMR spectra
451 were recorded at the Danish National Instrument Centre for NMR spectroscopy of Biological Macromolecules at the
452 Carlsberg Laboratory. Maja Tenkanen (University of Helsinki) is thanked for doubly substituted AXOS.

453

454 **Compliance with Ethical Standards**

455

456 Funding: This work is supported by the Danish Council for Independent Research | Natural Sciences (FNU) [grant
457 number 09-072151], by 1/3 PhD fellowship from the Technical University of Denmark (to CW) and by a Hans
458 Christian Ørsted postdoctoral fellowship from DTU (to DC).

459

460 Ethical approval: This article does not contain any studies with human participants or animals performed by any of the
461 authors.

462
463 Conflict of interest: Barry McCleary is CEO and founder of Megazyme International.

464
465 **References**

- 466 Barkholt V, Jensen AL (1989) Amino acid analysis: determination of cysteine plus half-cystine in proteins after
467 hydrochloric acid hydrolysis with a disulfide compound as additive. *Anal Biochem* 177:318–322. doi:
468 10.1016/0003-2697(89)90059-6
- 469 Bauer S, Vasu P, Persson S, Mort AJ, Somerville CR (2006) Development and application of a suite of polysaccharide-
470 degrading enzymes for analyzing plant cell walls. *Proc Natl Acad Sci U S A* 103:11417–11422. doi:
471 10.1073/pnas.0604632103
- 472 Bowman MJ, Dien BS, Vermillion KE, Mertens JA. (2015) Isolation and characterization of unhydrolyzed
473 oligosaccharides from switchgrass (*Panicum virgatum*, L.) xylan after exhaustive enzymatic treatment with
474 commercial enzyme preparations. *Carbohydr Res* 407:42–50. doi: 10.1016/j.carres.2015.01.018
- 475 Britton HTS, Robinson RA (1931) Universal buffer solutions and the dissociation constant of veronal. *J Chem Soc*
476 1456–1462. doi: 10.1039/jr9310001456
- 477 Bromley JR, Busse-Wicher M, Tryfona T, Mortimer JC, Zhang Z, Brown DM, Dupree P (2013) GUX1 and GUX2
478 glucuronyltransferases decorate distinct domains of glucuronoxylan with different substitution patterns. *Plant J*
479 74:423–434. doi: 10.1111/tpj.12135
- 480 Buchan DWA, Ward SM, Lobley AE, Nugent TCO, Bryson K, Jones DT (2010) Protein annotation and modelling
481 servers at University College London. *Nucleic Acids Res* 38:563–568. doi: 10.1093/nar/gkq427
- 482 Busk PK, Lange L (2013) Function-based classification of carbohydrate-active enzymes by recognition of short,
483 conserved peptide motifs. *Appl Environ Microbiol* 79:3380–3391. doi: 10.1128/AEM.03803-12
- 484 Couturier M, Haon M, Coutinho PM, Henrissat B, Lesage-Meessen L, Berrin J-G (2011) *Podospora anserina*
485 hemicellulases potentiate the *Trichoderma reesei* secretome for saccharification of lignocellulosic biomass. *Appl*
486 *Environ Microbiol* 77:237–246. doi: 10.1128/AEM.01761-10
- 487 Cuyvers S, Dornez E, Rezaei MN, Pollet A, Delcour JA, Courtin CM (2011) Secondary substrate binding strongly
488 affects activity and binding affinity of *Bacillus subtilis* and *Aspergillus niger* GH11 xylanases. *FEBS J* 278:1098–
489 1111. doi: 10.1111/j.1742-4658.2011.08023.x
- 490 De La Mare M, Guais O, Bonnin E, Weber J, Francois JM (2013) Molecular and biochemical characterization of three
491 GH62 α -L-arabinofuranosidases from the soil deuteromycete *Penicillium funiculosum*. *Enzyme Microb Technol*
492 53:351–358. doi: 10.1016/j.enzmictec.2013.07.008
- 493 De Vos D, Collins T, Nerinckx W, Savvides SN, Claeysens M, Gerday C, Feller G, Van Beeumen J (2006)
494 Oligosaccharide binding in family 8 glycosidases: crystal structures of active-site mutants of the β -1,4-xylanase
495 pXyl from *Pseudoaltermonas haloplanktis* TAH3a in complex with substrate and product. *Biochemistry*
496 45:4797–4807. doi: 10.1021/bi052193e
- 497 Emanuelsson O, Brunak S, von Heijne G, Nielsen H (2007) Locating proteins in the cell using TargetP, SignalP and
498 related tools. *Nat Protoc* 2:953–971. doi: 10.1038/nprot.2007.131

499 Goubet F, Jackson P, Deery MJ, Dupree P (2002) Polysaccharide analysis using carbohydrate gel electrophoresis: a
500 method to study plant cell wall polysaccharides and polysaccharide hydrolases. *Anal Biochem* 300:53–68. doi:
501 10.1006/abio.2001.5444

502 Hashimoto K, Yoshida M, Hasumi K (2011) Isolation and characterization of CcAbf62A, a GH62 α -L-
503 arabinofuranosidase, from the Basidiomycete *Coprinopsis cinerea*. *Biosci Biotechnol Biochem* 75:342–345. doi:
504 10.1271/bbb.100434

505 Jordan DB, Bowman MJ, Braker JD, Dien BS, Hector RE, Lee CC, Mertens JA, Wagschal K (2012) Plant cell walls to
506 ethanol. *Biochem J* 442:241–252. doi: 10.1042/BJ20111922

507 Kaur AP, Nocek BP, Xu X, Lowden MJ, Leyva JF, Stogios PJ, Cui H, Di Leo R, Powlowski J, Tsang A, Savchenko A
508 (2014) Functional and structural diversity in GH62 α -L-arabinofuranosidases from the thermophilic fungus
509 *Scytalidium thermophilum*. *Microbiol Biotechnol*. 8:419–433 doi: 10.1111/1751-7915.12168

510 Kellett LE, Poole DM, Ferreira LM, Durrant AJ, Hazlewood GP, Gilbert HJ (1990) Xylanase B and an
511 arabinofuranosidase from *Pseudomonas fluorescens* subsp. *cellulosa* contain identical cellulose-binding domains
512 and are encoded by adjacent genes. *Biochem J* 272:369–376.

513 Kimura I, Yoshioka N, Kimura Y, Tajima S (2000) Cloning, sequencing and expression of an α -L-arabinofuranosidase
514 from *Aspergillus sojae*. *J Biosci Bioeng* 89:262–266.

515 Lange L, Sørensen HR, Hamann T (2006) New *Penicillium* arabinofuranosidase, used in dough and useful ethanol
516 process, mashing process, and for producing feed composition. WO2006/125438-A1

517 Li W, Cowley A, Uludag M, Gur T, McWilliam H, Squizzato S, Park YM, Buso N, Lopez R (2015) The EMBL-EBI
518 bioinformatics web and programmatic tools framework. *Nucleic Acids Res* 43:580–584. doi: 10.1093/nar/gkv279

519 Lombard V, Golaconda Ramulu H, Drula E, Coutinho PM, Henrissat B (2014) The carbohydrate-active enzymes
520 database (CAZy) in 2013. *Nucleic Acids Res* 42:D490–495. doi: 10.1093/nar/gkt1178

521 Ludwiczek ML, Heller M, Kantner T, McIntosh LP (2007) A secondary xylan-binding site enhances the catalytic
522 activity of a single-domain family 11 glycoside hydrolase. *J Mol Biol* 373:337–354. doi:
523 10.1016/j.jmb.2007.07.057

524 Maehara T, Fujimoto Z, Ichinose H, Michikawa M, Harazono K, Kaneko S (2014) Crystal structure and
525 characterization of the glycoside hydrolase family 62 α -L-arabinofuranosidase from *Streptomyces coelicolor*. *J*
526 *Biol Chem* 289:7962–7972. doi: 10.1074/jbc.M113.540542

527 Marchler-Bauer A, Lu S (2011) CDD: a Conserved Domain Database for the functional annotation of proteins. *Nucleic*
528 *Acids Res* 39:D225–D229. doi: 10.1093/nar/gkq1189

529 Margolles-Clark E, Tenkanen M, Nakari-Setälä T, Penttilä M (1996) Cloning of genes encoding α -L-
530 arabinofuranosidase and β -xylosidase from *Trichoderma reesei* by expression in *Saccharomyces cerevisiae*. *Appl*
531 *Environ Microbiol* 62:3840–3846.

532 McCleary BV, McKie VA, Draga A, Rooney E, Mangan D, Larkin J (2015) Hydrolysis of wheat flour arabinoxylan,
533 acid-debranched wheat flour arabinoxylan and arabino-xylo-oligosaccharides by β -xylanase, α -L-
534 arabinofuranosidase and β -xylosidase. *Carbohydr Res* 407:79–96 doi: 10.1016/j.carres.2015.01.017

535 McKee LS, Peña MJ, Rogowski A, Jackson A, Lewis RJ, York WS, Krogh KBRM, Viksø-Nielsen A, Skjøl M, Gilbert
536 HJ, Marles-Wright J (2012) Introducing endo-xylanase activity into an exo-acting arabinofuranosidase that targets
537 side chains. *Proc Natl Acad Sci U S A* 109:6537–6542. doi: 10.1073/pnas.1117686109

538 McKie VA, Black GW, Millward-Sadler SJ, Hazlewood GP, Laurie JI, Gilbert HJ (1997) Arabinase A from
539 *Pseudomonas fluorescens* subsp. *cellulosa* exhibits both an endo- and an exo- mode of action. *Biochem J*
540 555:547–555. doi: 10.1042/bj3230547

541 Mohun AF, Cook IJ (1962) An improved dinitrosalicylic acid method for determining blood and cerebrospinal fluid
542 sugar levels. *J Clin Pathol* 15:169–180. doi: 10.1136/jcp.15.2.169

543 Nielsen JW, Kramhøft B, Bozonnet S, Abou Hachem M, Stipp SLS, Svensson B, Willemoës M (2012) Degradation of
544 the starch components amylopectin and amylose by barley α -amylase 1: role of surface binding site 2. *Arch*
545 *Biochem Biophys* 528:1–6. doi: 10.1016/j.abb.2012.08.005

546 Numan MT, Bhosle NB (2006) α -L-arabinofuranosidases: the potential applications in biotechnology. *J Ind Microbiol*
547 *Biotechnol* 33:247–260. doi: 10.1007/s10295-005-0072-1

548 Nurizzo D, Turkenburg JP, Charnock SJ, Roberts SM, Dodson EJ, McKie VA, Taylor EJ, Gilbert HJ, Davies GJ (2002)
549 *Cellvibrio japonicus* α -L-arabinanase 43A has a novel five-blade beta-propeller fold. *Nat Struct Biol* 9:665–668.
550 doi: 10.1038/nsb835

551 Oudjeriouat N, Moreau Y, Santimone M, Svensson B, Marchis-Mouren G, Desseaux V (2003) On the mechanism of α -
552 amylase. *Eur J Biochem* 270:3871–3879. doi: 10.1046/j.1432-1033.2003.03733.x

553 Pitkänen L, Virkki L, Tenkanen M, Tuomainen P (2009) Comprehensive multidetector HPSEC study on solution
554 properties of cereal arabinoxylans in aqueous and DMSO solutions. *Biomacromolecules* 10:1962–1969. doi:
555 10.1021/bm9003767

556 Pitson SM, Voragen AG, Beldman G (1996) Stereochemical course of hydrolysis catalyzed by arabinofuranosyl
557 hydrolases. *FEBS Lett* 398:7–11. doi: http://dx.doi.org/10.1016/S0014-5793(96)01153-2

558 Poutanen K (1988) An α -L-arabinofuranosidase of *Trichoderma reesei*. *J Biotechnol* 7:271–281. doi: 10.1016/0168-
559 1656(88)90039-9

560 Ransom RF, Walton JD (1997) Purification and characterization of extracellular β -xylosidase and α -arabinosidase from
561 the plant pathogenic fungus *Cochliobolus carbonum*. *Carbohydr Res* 297:357–364. doi: 10.1016/S0008-
562 6215(96)00281-9

563 Sakamoto T, Ogura A, Inui M, Tokuda S, Hosokawa S, Ihara H, Kasai N (2010) Identification of a GH62 α -L-
564 arabinofuranosidase specific for arabinoxylan produced by *Penicillium chrysogenum*. *Appl Microbiol Biotechnol*
565 90:137–146. doi: 10.1007/s00253-010-2988-2

566 Sakamoto T, Inui M, Yasui K, Hosokawa S, Ihara H (2013) Substrate specificity and gene expression of two
567 *Penicillium chrysogenum* α -L-arabinofuranosidases (AFQ1 and AFS1) belonging to glycoside hydrolase families
568 51 and 54. *Appl Microbiol Biotechnol* 97:1121–1130. doi: 10.1007/s00253-012-3978-3

569 Schmidt A, Gu GM, Kratky C (1999) Xylan binding subsite mapping in the xylanase from *Penicillium simplicissimum*
570 using xylooligosaccharides as cryo-protectant. *Biochemistry* 38:2403–2412. doi: 10.1021/bi9821081

571 Siguier B, Haon M, Nahoum V, Marcellin M, Burette-Schiltz O, Coutinho PM, Henrissat B, Mourey L, O Donohue MJ,
572 Berrin J-G, Tranier S, Dumon C (2014) First structural insights into α -L-arabinofuranosidases from the two GH62
573 glycoside hydrolase subfamilies. *J Biol Chem* 289:5261–5273. doi: 10.1074/jbc.M113.528133

574 Söding J, Biegert A, Lupas AN (2005) The HHpred interactive server for protein homology detection and structure
575 prediction. *Nucleic Acids Res* 33:244–248. doi: 10.1093/nar/gki408

576 Tamura K, Stecher G, Peterson D, Filipski A, Kumar S (2013) MEGA6: Molecular evolutionary genetics analysis

577 version 6.0. Mol Biol Evol 30:2725–2729. doi: 10.1093/molbev/mst197
578 Tsujibo H, Takada C, Wakamatsu Y, Kosaka M, Tsuji A, Miyamoto K, Inamori Y (2002) Cloning and expression of an
579 α -L-arabinofuranosidase gene (*stxIV*) from *Streptomyces thermoviolaceus* OPC-520, and characterization of the
580 enzyme. Biosci Biotechnol Biochem 66:434–438. doi: <http://doi.org/10.1271/bbb.66.434>
581 Van Laere KMJ, Voragen CHL, Kroef T, Van den Broek LAM, Beldman G, Vorage, Paper O (1999) Purification and
582 mode of action of two different arabinoxylan arabinofuranohydrolases from *Bifidobacterium adolescentis* DSM
583 20083. Appl Microbiol Biotechnol 51:606–613. doi: 10.1007/s002530051439
584 Vandermarliere E, Bourgois TM, Rombouts S, Van Campenhout S, Volckaert G, Strelkov SV, Delcour JA, Rabijns A,
585 Courtin CM (2008) Crystallographic analysis shows substrate binding at the -3 to +1 active-site subsites and at
586 the surface of glycoside hydrolase family 11 endo-1,4- β -xylanases. Biochem J 410:71–79. doi:
587 10.1042/BJ20071128
588 Vincent P, Shareck F, Dupont C, Morosoli R, Kluepfel D (1997) New α -L-arabinofuranosidase produced by
589 *Streptomyces lividans*: cloning and DNA sequence of the *abfB* gene and characterization of the enzyme. 852:845–
590 852. doi: 10.1042/bj3220845
591 Wallner B, Elofsson A (2003) Can correct protein models be identified? Protein Sci 12:1073–1086. doi:
592 10.1110/ps.0236803.a
593 Wang W, Mai-Gisoni G, Stogios PJ, Kaur A, Xu X, Cui H, Turunen O, Savchenko A, Master ER (2014) Elucidation
594 of the molecular basis for arabinoxylan-debranching activity of a thermostable family GH62 α -L-
595 arabinofuranosidase from *Streptomyces thermoviolaceus*. Appl Environ Microbiol 80:5317–5329. doi:
596 10.1128/AEM.00685-14
597

598

599

600

601

602

603

604

605

606

607

608

609

610 **TABLES**611 Table 1: Specific activities for *AnAbf62A-m2,3*

Substrate	Specific activity (U/mg)
Wheat arabinoxylan	67.42 ± 4.53 (1.00)
Rye arabinoxylan	64.24 ± 1.82 (0.95)
Oat spelt xylan	49.14 ± 1.19 (0.73)
Birchwood xylan	n.d.
Barley β-glucan	n.d.
Sugar beet L-arabinan	1.43 ± 0.14 (0.02)
Linear L-arabinan	n.d.
Larch wood arabinogalactan	0.08 ± 0.01 (0.001)
Acacia tree gum arabic	0.25 ± 0.02 (0.003)
4-nitrophenyl α-L-arabinofuranoside	1.66 ± 0.24 (0.02)
4-nitrophenyl β-D-xylopyranoside	0.03 ± 0.01 (0.0004)
4-nitrophenyl α-L-arabinopyranoside	0.04 ± 0.01 (0.001)
A ³ X	37 ± 1.1 (0.55)
A ² XX	59 ± 0.5 (0.88)
A ² XX+A ³ XX (7:3)	80 ± 2.1 (1.19)
XA ² XX+XA ³ XX (1:1)	80 ± 3.5 (1.19)
A ²⁺³ XX	n.d.

612 n.d., not detected. Relative values are in parentheses. All experiments were done in triplicates.

613 Table 2: Kinetic parameters for hydrolysis of wheat arabinoxylan, sugar beet L-arabinan and 4-nitrophenyl α -L-arabinofuranoside by *AnAbf62A*-m2,3 wild-type and
 614 catalytic site (D28A, D136A and E188A) and putative SBS (W23A, Y44A and W23A/Y44A) mutants.

Wheat arabinoxylan	Wild-type	D28A	D136A	E188A	W23A	Y44A	W23A/Y44A
k_{cat} (s^{-1})	178 \pm 26 (1.00)	0.64 \pm 0.06 (0.00)	0.63 \pm 0.09 (0.00)	n.d	52.11 \pm 9.25 (0.29)	46.54 \pm 3.16 (0.26)	80.21 \pm 10.53 (0.45)
K_{m} ($\text{mg}\times\text{ml}^{-1}$)	4.90 \pm 0.91 (1.00)	2.62 \pm 0.05 (0.53)	1.57 \pm 0.32 (0.32)	n.d.	2.35 \pm 0.63 (0.48)	1.02 \pm 0.13 (0.21)	6.93 \pm 1.15 (1.41)
$k_{\text{cat}}/K_{\text{m}}$ ($\text{s}^{-1}\times\text{mM}^{-1}$)	36.37 (1.00)	0.24 (0.01)	0.40 (0.01)	n.d	22.18 (0.61)	45.76 (1.26)	11.56 (0.32)
Specific activity ($\text{U}\times\text{mg}^{-1}$)	67.42 \pm 4.53 (1.00)	0.52 \pm 0.02 (0.01)	0.41 \pm 0.02 (0.01)	0.04 \pm 0.00 (0.00)	48.29 \pm 6.98 (0.72)	45.82 \pm 2.05 (0.68)	50.63 \pm 3.26 (0.75)
K_{i} ($\text{mg}\times\text{ml}^{-1}$)	2.89 \pm 0.58 (1.00)	-	6.0 \pm 1.50 (2.08)	-	16.32 \pm 8.51 (5.64)	11.89 \pm 2.19 (4.11)	19.71 \pm 7.68 (6.82)
Sugar beet L-arabinan	Wild-type	D28A	D136A	E188A	W23A	Y44A	W23A/Y44A
k_{cat} (s^{-1})	1.03 \pm 0.03 (1.00)	-	-	-	0.73 \pm 0.02 (0.71)	0.96 \pm 0.02 (0.93)	0.81 \pm 0.04 (0.79)
K_{m} ($\text{mg}\times\text{ml}^{-1}$)	15.63 \pm 1.25 (1.00)	-	-	-	20.60 \pm 1.72 (1.32)	12.03 \pm 0.79 (0.77)	33.78 \pm 3.47 (2.16)
$k_{\text{cat}}/K_{\text{m}}$ ($\text{s}^{-1}\times\text{mM}^{-1}$)	0.07 (1.00)	-	-	-	0.04 (0.57)	0.08 (1.14)	0.02 (0.29)
Specific activity ($\text{U}\times\text{mg}^{-1}$)	1.43 \pm 0.14 (1.00)	-	-	-	1.06 \pm 0.08 (0.74)	0.77 \pm 0.08 (0.54)	1.07 \pm 0.01 (0.75)
4-nitrophenyl α -L-arabinofuranoside	Wild-type	D28A	D136A	E188A	W23A	Y44A	W23A/Y44A
$k_{\text{cat}}/K_{\text{m}}$ ($\text{s}^{-1}\times\text{mM}^{-1}$)	0.26 \pm 0.01 (1.00)	-	-	-	0.17 \pm 0.00 (0.65)	0.21 \pm 0.02 (0.81)	0.27 \pm 0.01 (1.04)
Specific activity ($\text{U}\times\text{mg}^{-1}$)	1.66 \pm 0.24 (1.00)	-	-	-	1.28 \pm 0.03 (0.77)	2.42 \pm 0.08 (1.46)	1.99 \pm 0.12 (1.20)

615 n.d. - not measured. Relative values are in parentheses. All experiments were in triplicates.

616 Table 3: Relative activities on arabinoxylooligosaccharides for *AnAbf62A*-m2,3 wild-type and mutants of the putative
 617 SBS

AXOS*	Wild-type	W23A	Y44A	W23A/Y44A
A ³ X	1.00	0.04	0.03	0.04
A ² XX+XA ³ X+A ³ XX	1.00	0.12	0.10	0.11
XA ² XX+XA ³ XX	1.00	0.25	0.18	0.23

618 All experiments were in triplicates.

619
 620
 621
 622
 623
 624
 625
 626
 627
 628
 629
 630
 631
 632
 633
 634
 635
 636
 637
 638
 639
 640
 641
 642
 643
 644
 645
 646
 647
 648
 649
 650

651 **FIGURE LEGENDS**

652 **Fig. 1** Structural homology model of *AnAbf62A*-m2,3 overlaid with xylopentaose (cyan) from *ScAbf62A* (PDB ID
653 3WN2) and arabinose (orange) from *UmAbf62A* (PDB ID 4N2R). Subsites are labelled according to McKee et al.
654 (2012). The catalytic residues are light purple and the putative surface binding site residues in dark purple.

655
656 **Fig. 2** Subsites and side chains shown to interact with xylooligosaccharides in crystal structures of *SthAbf62A* (PDB ID
657 4O8O) (pink), *StAbf62C* (PDB ID 4PVI) (brown) *UmAbf62A* (PDB ID 4N2R) (green), *PaAbf62A* (PDB ID 4N2Z)
658 (salmon) and *ScAbf62A* (PDB ID 3WN2) (yellow). Only side chains that differ from *AnAbf62A*-m2,3 (grey) are
659 included for the above mentioned. Xylopentaose (cyan) from *ScAbf62A* (PDB ID 3WN2) and arabinose (orange) from
660 *SthAbf62A* (PDB ID 4O8O) are shown. Numbering refers to *AnAbf62A*-m2,3.

661
662 **Fig. 3** Affinity gel electrophoresis of *AnAbf62A*-m2,3. A) 17 h run with 0.05 % wheat arabinoxylan, B) control
663 (without polysaccharide) and with 0.001 % C) wheat arabinoxylan, D) oat spelt xylan, E) birchwood xylan, F) barley β -
664 glucan, G) sugar beet L-arabinan, H) acacia tree gum arabic and I) larch arabinogalactan. Lane 1: marker; lane 2: wild-
665 type; lane 3: W23A; lane 4: Y44A; lane 5: W23A/Y44A. The lower vertical line shows the migration of *AnAbfGH62A*-
666 m2,3 wild-type in the control gel without polysaccharide and the upper one shows a marker used to align the gels.

667
668 **Fig. 4** Substrate hydrolysis curves by *AnAbf62A*-m2,3 of A) wheat arabinoxylan, B) sugar beet L-arabinan, C) wheat
669 arabinoxylan by catalytic site mutants and D) 4-nitrophenyl α -L-arabinofuranoside. *AnAbf62A*-m2,3 wild-type (●),
670 W23A (■), Y44A (○), W23A/Y44A (□), D28A (▲) and D136A (▼).

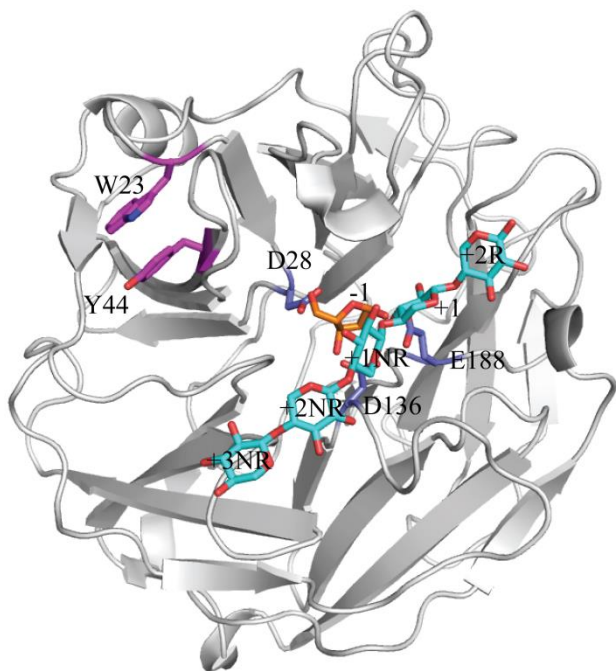
671
672 **Fig. 5** Time course of hydrolysis by *AnAbf62A*-m2,3 of AXOS (1:1 molar ratio of β -D-Xylp-(1 \rightarrow 4)-[α -L-Araf-(1 \rightarrow 2)]-
673 β -D-Xylp-(1 \rightarrow 4)- β -D-Xylp-(1 \rightarrow 4)- β -D-Xylp (A²XX) and β -D-Xylp-(1 \rightarrow 4)-[α -L-Araf-(1 \rightarrow 3)]- β -D-Xylp-(1 \rightarrow 4)- β -D-
674 Xylp-(1 \rightarrow 4)- β -D-Xylp (A³XX) by *AnAbf62A*-m2,3 monitored by ¹H NMR spectroscopy. Peak area integration values
675 are shown for the signals from 1,3-linked arabinofuranose (○), 1,2-linked arabinofuranose (●), and arabinose on β -
676 furanose (▼), α -furanose (Δ), α -pyranose (■) and β -pyranose (□) forms, respectively.

677
678 **Fig. 6** Close-up surface representation of *AnAbf62A*-m2,3 putative surface binding site (SBS) situated Trp²³ and Tyr⁴⁴
679 (dark purple) with xylopentaose (cyan) from *ScAbf62A* (PDB ID 3WN2) and arabinose (orange) from *SthAbf62A*
680 (PDB ID 4O8O). A) End-view from subsite +3NR on the substrate binding crevice, B) Side-view on the substrate
681 binding crevice.

682
683
684
685
686
687
688
689

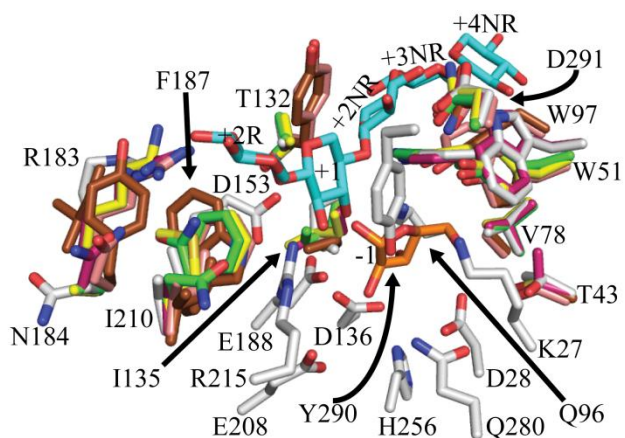
690 **FIGURES**

691 Fig. 1



692
693
694
695
696
697
698
699
700
701
702
703
704
705
706
707
708
709
710
711
712
713
714

715 Fig. 2



716

717

718

719

720

721

722

723

724

725

726

727

728

729

730

731

732

733

734

735

736

737

738

739

740

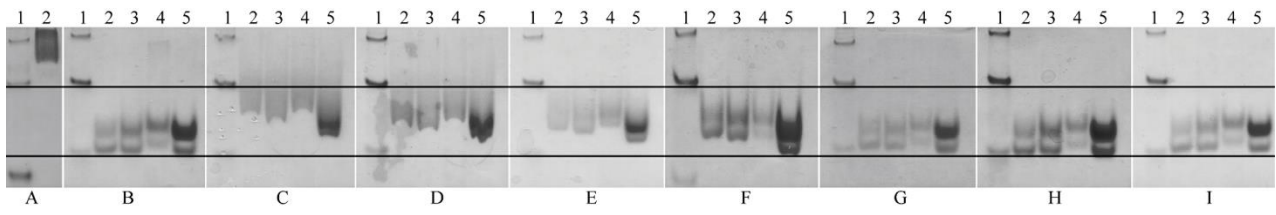
741

742

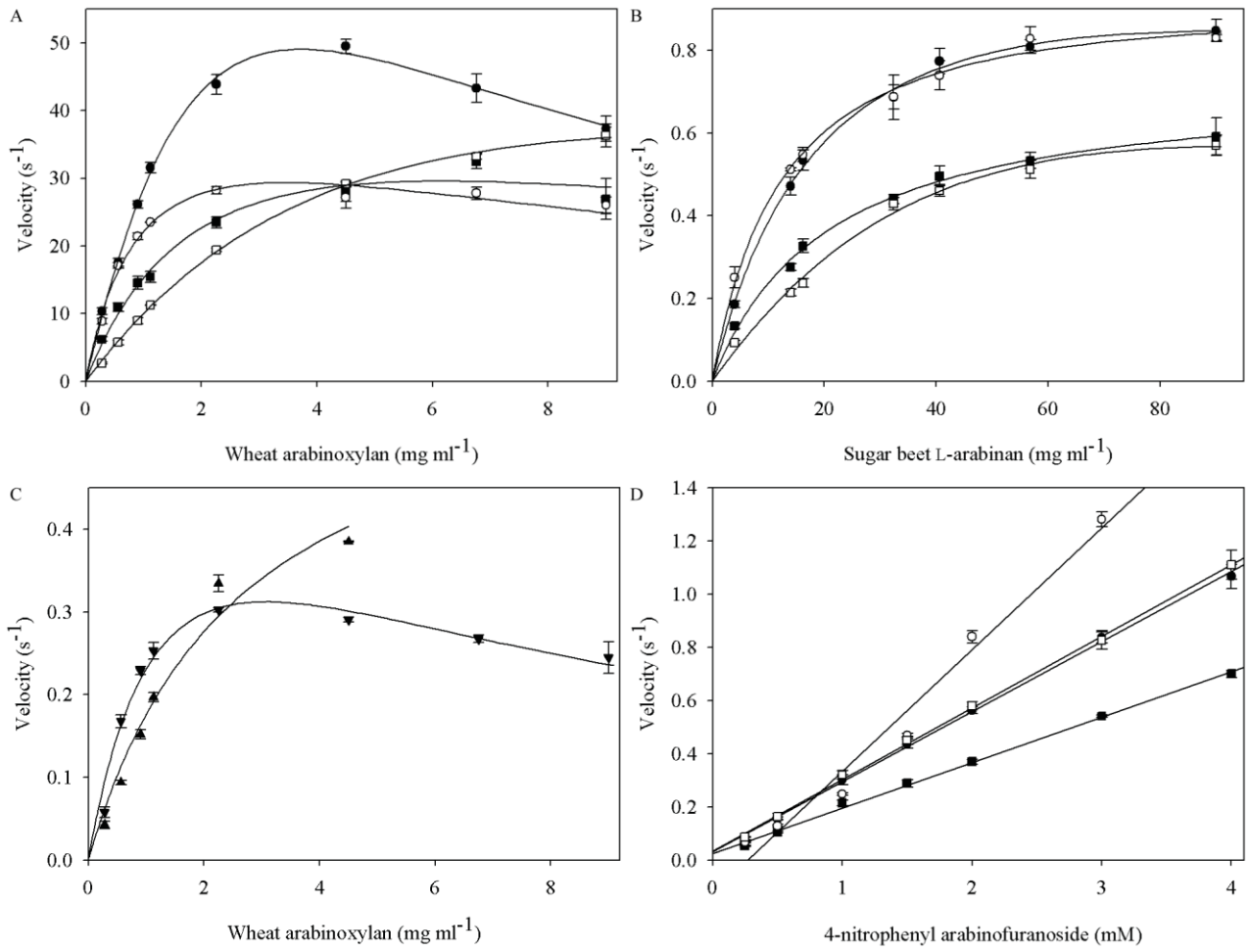
743

744

745 Fig. 3



780 Fig. 4



781

782

783

784

785

786

787

788

789

790

791

792

793

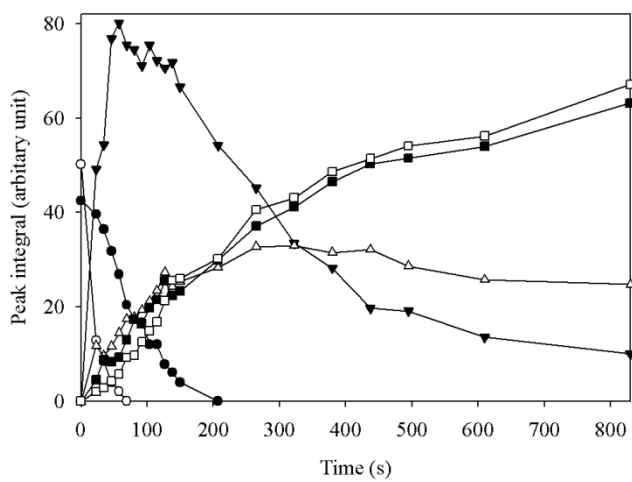
794

795

796

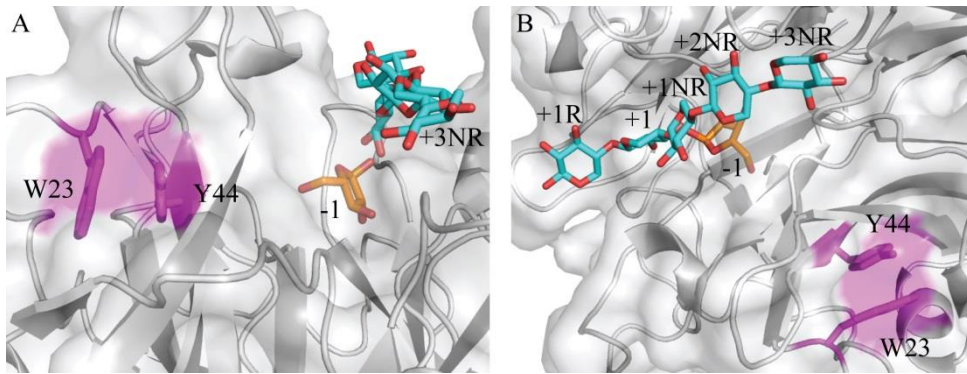
797

798 Fig. 5



799
800
801
802
803
804
805
806
807
808
809
810
811
812
813
814
815
816
817
818
819
820
821
822
823
824
825
826

827 Fig. 6



828

829

830

831

832